Check for updates

Bandwidth enhancement of a planar SIW cavity-backed slot antenna using slot and metallic-shorting via

Divya Chaturvedi[1] · Ayman A. Althuwayb[2] · Arvind Kumar[3]

Abstract

A bandwidth enhancement method has been described in this paper by using the various cavity modes. The cavity is achieved by a wisely developed substrate integrated waveguide (SIW) technology, which realizes a non-planar cavity-backed antenna in planar form. The whole antenna circuit and feed are integrated on the same plane. Rather than using a conventional slot, a dual T-shaped slot is preferred as a radiating element. The combination of dual T-shaped slot and a shorting via enhances the bandwidth. The slot yields three resonances due to TE_{110} mode and modified TE_{120}/TE_{130} modes. The placement of shorting via modifies TE_{110} mode, which gets coupled with the other higher-order modes and enhances the bandwidth by 50%. The footprint of the square SIW cavity of antenna is $0.86\lambda_g \times 0.86\lambda_g$ mm^2. The proposed geometry is prototyped and experimentally tested. The antenna covers a bandwidth of 400 MHz (6.75–7.15 GHz) with gain of 5.5–6.1 dBi. The antenna shows a front-to-back ratio better than 15 dB with a unidirectional radiation pattern and the cross-polar level below -15 dB. The antenna is fabricated on a thin substrate of profile $0.052\lambda_g$ on a single layer. In addition, the proposed structure possesses the advantages of low profile, planar, compact size with flat gain and uniform radiation features.

Keywords Bandwidth-enhancement · Cavity-backed antenna · Dual-T shaped slot · Shorting via · Substrate integrated waveguide

1 Introduction

In recent years, the demand for multi-band communication devices has been increasing rapidly with the progression in wireless technologies. With this advancement, the planar low-cost multi-band antennas of compact size have been becoming very popular nowadays [1–4]. For point-to-point communication, the antenna should have a unidirectional radiation pattern, a high front-to-back ratio, and better isolation from the surrounding. The conventional slot antenna based on micro-strip technology offers low profile

configuration, however, it suffers from bidirectional radiation pattern and relatively poorer isolation [5–7].

Substrate integrates waveguide (SIW) cavity technique has emerged in the last decade with overwhelming applications and innovative ways to approach the existing applications. With the influx of the SIW, co-design of an antenna and its associate circuitry on same plane becomes more reliable, unlike traditional circuitry will consume little board area [8–10]. Moreover, it minimizes unwanted surface losses, while delivering a high-power handling capacity. This is where the SIW comes in, though there are many different types of designs out in the available literature. By the virtue of the SIW cavity-backing structure, the undesired surface current at the edge of the ground plane and the back lobe radiation has reduced significantly. Thus, it expands the antenna gain with a low-profile configuration and high performance to price ratio. The conventional SIW cavity-backed slot antennas suffer from the problem of narrow operating bandwidth and bulky size. Various methods have been explored over the years by researchers to enhance the bandwidth of the SIW cavity-backed slot antenna. The bandwidth is enlarged by exciting two hybrid modes in proximity. The cavity modes are tuned

✉ Ayman A. Althuwayb
aaalthuwayb@ju.edu.sa

1 Department of Electronics and Communication Engineering, SRM University, Amravati, AP, India

2 Department of Electrical Engineering, College of Engineering, Jouf University, Sakaka 72388, Aljouf, Saudi Arabia

3 School of Electronics Engineering, Vellore Institute of Technology, Vellore, India

for by optimizing the dimensions of the cavity, location, and dimensions of the slot [11, 12]. A dual bowtie split ring resonator slot-cu-via is opted in [13], the position of the shorting via is optimized just above the slot to excite a hybrid mode in [14], the longitudinal and transverse slotted radiator with shorted vias [15].

A circular ring slot is used for radiation, which produces the cavity mode and the slot mode in [16], the cavity modes are coupled in the desired band by using tilted slots with shorting vias in [17]. Half-mode (HM) SIW cavity backing antenna in a compact size was presented in [18]. The dominant mode of the cavity and patch are coupled in [19], a square ring slot is used in [20], a modified triangular ring slot is etched nearby one corner of the cavity [21], half-and quarter-modes of SIW cavities are coupled in 60 GHz frequency band [22], a wideband is obtained for Wi-Fi applications by coupling hybrid modes using multiple slots sections in [23]. Later, a coplanar-waveguide-fed planar integrated cavity-backed slotted antenna was presented in [24], where the radiation mechanism was realized with the help of higher-order 3×3 mode. Half-mode/quarter-mode substrate integrated waveguide-based wideband antenna design process was suggested for millimeter-wave application in [25]. Enhanced impedance bandwidth was realized by incorporating multi-layered substrate configuration [26, 27]. But multi-layered configuration increases the fabrication complexity. Furthermore, different design with improved bandwidth performance was presented in [28–30]. The above-mentioned antennas demonstrate various ways to enhance the bandwidth, however, limited antennas are available which offer larger bandwidth with higher gain in a compact size planar configuration. This article illustrates a compact, low-profile SIW cavity-backed slot antenna designing, analysis, and development.

The antenna comprises a dual T-shaped slot and a shorting via located between the slots. The shorting via is mainly placed to enlarge the bandwidth, along it offers better impedance matching. The antenna covers the bandwidth in the range of 6.8–7.25 GHz with a fractional bandwidth of 6.5%. An inset microstrip feed is used for excitation of modes, which also offers a simple transition of feed to cavity aperture. The proposed antenna offers the combined benefits of both non-planar cavity-backed antenna (i.e., lower losses with higher power handling ability and lower surface current) and the planar slot antennas (low profile, easy manufacturing, and planar form). The proposed antenna is simple and cost-effective since the overall geometry is realized in a compact- single-layered structure.

2 Design and principle of operation

The design of the proposed SIW cavity-backed slot antenna is illustrated in Fig. 1. It comprises a square SIW cavity, which is constructed by embedding rows of metal vias in a square fashion. The dimensions of the cavity are selected from the equations suggested in [4–6], which excite TE_{120} around 8.2 GHz. The SIW cavity is formed by embedding the metal posts in the dielectric substrate which forms the lateral conducting walls. The diameter (d) and pitch of metallic vias (s) are selected, $d/s \geq 0.5$ and $d/\lambda_o \leq 0.1$, to safeguard minimum loss of energy from the sidewalls of the cavity [31–33]. When the cavity is fed by an inset microstrip. feed, it resonates at 5.25, 8.3, and 8.85 GHz due to TE_{110}, TE_{120}, and TE_{130} modes, respectively. A dual T-shaped radiating slot has been engraved in the center of the top cladding of the cavity at $3\lambda_g$ distance from the upper/lower sidewalls of the cavity and $2\lambda_g$ distance from the left/right sidewalls of the cavity, where λ_g is the guiding wavelength at 8.2 GHz. The placement of the slot affects the current path of all the three modes significantly, hence the corresponding resonant
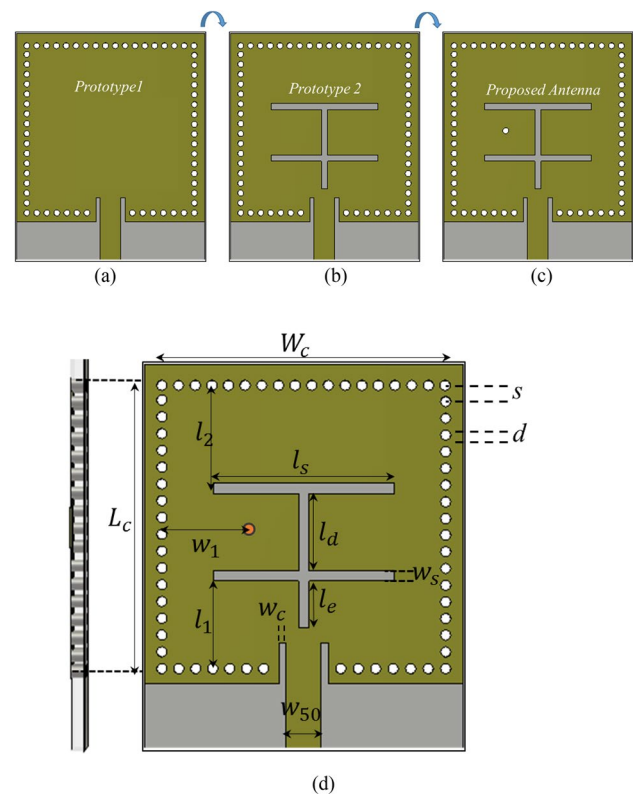

(a)   (b)   (c)

(d)

Fig. 1 Design evolution **a** *Prototype 1*: SIW cavity; **b** *Prototype 2*: cavity with slot; **c** *Proposed antenna*: cavity with slot and shorting via; **d** schematic diagram of proposed design, dimensions ($L_c = 27$, $W_c = 27$, $w_1 = 7.5$, $w_c = 0.7$, $w_s = 1$, $l_s = 17.5$, $l_1 = 10$, $l_2 = 9.6$, $s = 2$, $d = 1$, $w_{50} = 3.4$, $l_e = 4.5$, $l_d = 7.5$) (Units: mm)

frequencies shift towards the lower side around 4.8 GHz, 7 GHz, and 7.2 GHz due to the reactive loading effect of the slot which can be observed in Fig. 2b. This slot is a non-resonant type of length $1.5\lambda_g$ (where λ_g is the guide wavelength of the TE_{120} mode). The incorporation of the slot reduces series inductance, but at the same time adds the series capacitance in the cavity circuit [12]. The dual T-shaped slot varies the field distribution of TE_{120} mode and TE_{130} mode. Thus, modified TE_{120} and TE_{130} modes get excited in proximity. The dual T-shaped slot is placed at the center of the cavity to penetrate maximum for the TE_{120} mode. Hence, the placement of the slot does not affect the field profile of dominant mode, but it modifies the field distribution of TE_{120} mode as well as TE_{130} modes. The slot

increases the current path length for all the modes, which leads to decrease in operating frequencies. The slot is excited with the help of an inset microstrip feed, where the length l_f and width w_f of inset cuts are optimized in a way that load/antenna input impedance should be equal to the characteristic impedance of the feed so that perfect impedance matching can be achieved.

To further enlarge the bandwidth, a shorting via is placed carefully between the slots on one side of the cavity [14]. The location of the via is carefully selected where the maximum field of TE_{110} mode lies, while null for TE_{120} mode which can be observed from Fig. 3c. With the placement of via, the impedance matching is getting improved at all the resonances. The placement of the via reduces the current path length of TE_{110} mode approximately half, causes the shift in the resonant frequency towards the higher side. The modified TE_{120} mode is not affected by the via, however, the modified TE_{130} mode gets excited with better impedance matching at 7.15 GHz. Thus, by properly optimizing the position of the shorting via, all the three resonant frequencies are getting coupled within the frequency range of 6.78–7.22 GHz. The distance between shorting via and vias-wall 'w_1' affects the mode characteristics. When the via is moved away from the wall, the impedance matching improves and bandwidth correspondingly enlarged.
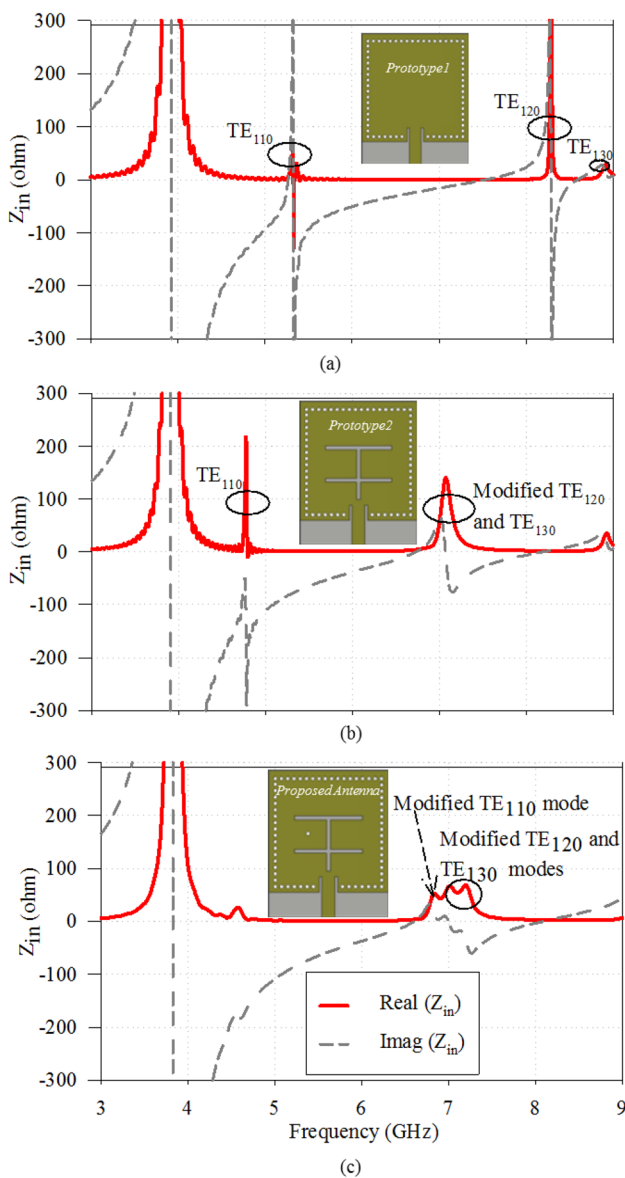

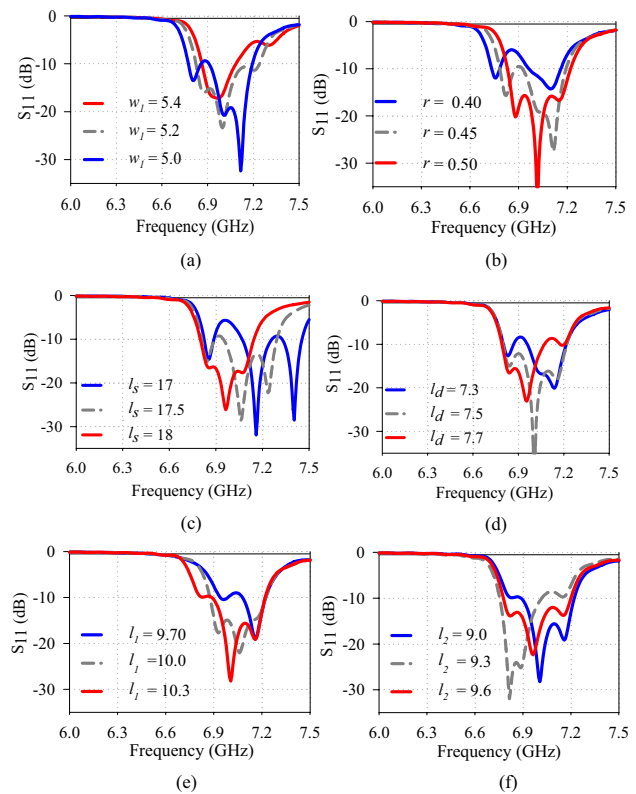**Fig. 2** Real (Z_{in}) and Imag. (Z_{in}) versus frequency plots

Fig. 3 Variation of the resonant frequency with different values of **a** w_1, **b** r, **c** l_s, **d** l_d, **e** l_1, and **f** l_2

Similar behavior can be observed by changing the radius 'r' of the shorting via. When the radius of the via increases, shunt inductance is getting increased, which enhances the impedance matching for all the modes, shown in Fig. 3b. The resonant frequency is always inversely proportional to the length of the slot 'l_s'. As the length of the slot increases, the area of perturbation is extending, which causes a strong reactive loading effect. Therefore, the resonant frequencies shift downward with 'l_s', displayed in Fig. 3c. The distance between the horizontal strips of the slots 'l_d' mainly affects modified TE_{120} and TE_{130} modes field distribution, which is evident from Fig. 3d. As the peak amplitude of E-field for TE_{120} and TE_{130} modes are getting penetrated more by the slots than TE_{110} mode. By optimizing the values of 'l_d', the return loss can be improved. The location of the dual T-slots from the sidewalls of the cavity also affects the mode characteristics. By varying the values of 'l_1' and 'l_2', the location of the slot changes, which directly affects the field distribution of the corresponding modes. By increasing 'l_1' and 'l_2', the return loss of all the modes is getting improved, due to which coupling of modes becomes stronger and bandwidth is getting enlarged. The vector electric field distribution has been displayed at each operating frequency in Fig. 4. The field distribution of modified TE_{110} mode, which is the fundamental mode shows even field distribution, resonates at 6.85 GHz. The modified TE_{120} mode has odd field distribution across the slot, resonates at 7 GHz while the modified TE_{130} mode resonates at 7.2 GHz. The E-field distribution of corresponding three modes has been displayed in Fig. 4a–c. The simulations have been performed by using CST Electromagnetic simulator 2018 based on the finite difference time domain (FDTD) method.

The reflection coefficients plot depends upon the various parameters, such as dimensions of the slot, location of the slot and via. By optimizing all the parameters, the modes are coupled and the standard − 10 dB impedance bandwidth is achieved as 424 MHz (6.78–7.22 GHz). The optimized
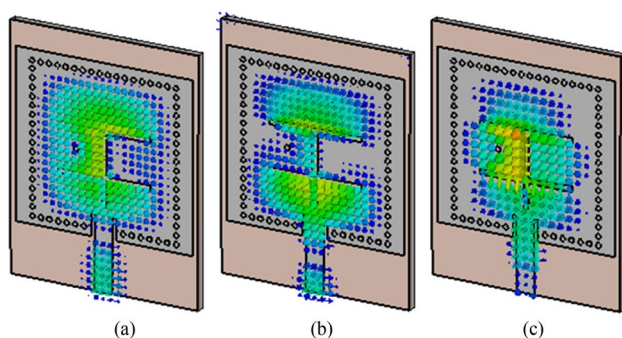
values of all the parameters are displayed in the caption of Fig. 1.

3 Measurement results

The variation of resonant frequencies against via dimensions as well as its position (r, w_1), slot length (l_s), distance between the slots (l_d), and slot positions (l_1, l_2), are discussed in the previous section. The optimized dimensions of the geometry have been obtained from the parametric studies and prototyped using the dielectric substrate of Rogers 5880 with loss tangent 0.001, dielectric permittivity of the material is 2.2 and thickness of the laminate is 1.57 mm. RT Duroid 5880 has been opted as the substrate of the proposed antenna as it is a well-established material. It has promising attributes of uniform electrical properties over wide frequency range, can be easily cut, shaped, machined to shape, and contains lowest electrical loss for reinforced PTFE material. With these properties, the dielectric losses of RT Duroid are very less at the operating frequency range compared to other existing materials in literature.

The antenna is fabricated using a simple printed circuit board (PCB) procedure and the vias are embedded by using plated through-hole (PTH) technique [11–17]. The Top and bottom view of the fabricated prototype is displayed in Fig. 5a, b, respectively. The size of the geometry in terms of
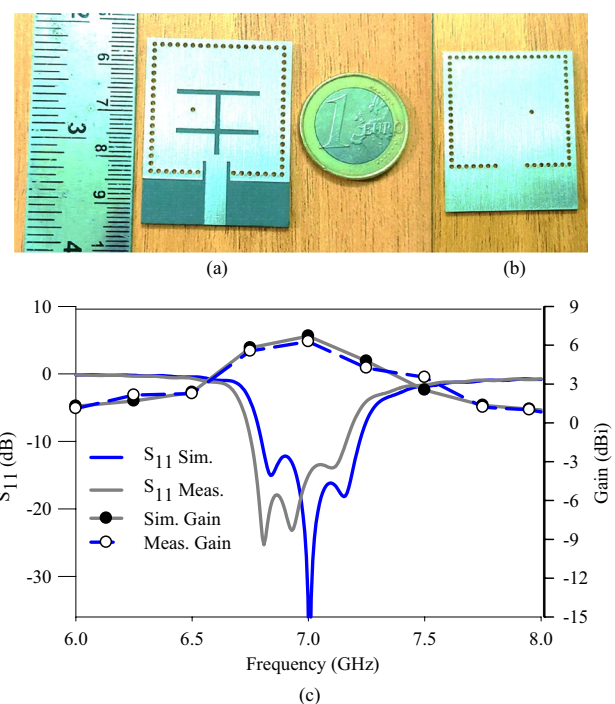

(a)   (b)

(c)

Fig. 5 Fabricated antenna: **a** top view, **b** bottom view, **c** |S_{11}|-parameter and gain plots vs frequency

(a)   (b)   (c)

Fig. 4 Vector electric field distribution at the top of the substrate: **a** modified TE_{110} mode at 6.85 GHz, **b** modified TE_{120} mode at 7.0 GHz and **c** modified TE_{310} mode at 7.2 GHz

guide wavelength at fundamental mode is $0.86\,\lambda_1 \times 0.86\,\lambda_1$. The proposed antenna possesses a low-profile single-layered structure of height as $0.052\,\lambda_1$.

The experimental results are measured in terms of return loss, directivity, and 2D radiation pattern. The return loss vs frequency is measured with the help of MS46122B 2-port vector network (VNA) analyzer. The simulated reflection coefficient below -10 dB covers the frequency range of 6.78–7.22 GHz (424 MHz) and the resonance frequency points at 6.85, 7, 7.2 GHz while the measured response slightly shifts towards the lower frequency band, covering the frequency range of 6.75–7.15 GHz (400 MHz) with resonance frequency points at 6.8, 6.92, 7.1 GHz. The slight discrepancy is possible due to insertion losses incorporated by the cables, probe, and end connectors. The gain is measured with a standard horn antenna. The measured gain closely follows the simulated gain response, displayed in Fig. 5c. The simulated gain varies in the range of 0.8–6.5 dBi, while the measured value of the gain varies in the range of 0.65–6.15 dBi. The peak value of the gain is observed at 7 GHz, which belongs to the modified TE_{120} mode. The gain is observed maximum for TE_{120} mode because the phase difference of plane waves is minimum in the far-field region for this specific mode. The slight discrepancy in the simulated and measured values of gain due to change in the conducting material properties. In simulations, the material is considered as perfect electric conductor (PEC) of ideal electrical conductivity while in fabricated prototype the coating of conducting material is used as Aluminum, which is having a finite electrical conductivity of 36.9×10^6 S/m. In general, pure aluminum is soft, ductile, and corrosion endurance, and having good electrical conductivity vs weight ratio. The total efficiency (i.e., including material and feeding losses) of the antenna varies between 78 and 88%. The peak efficiency is noticed around 7 GHz, i.e. 88%. Therefore, in the complete frequency range, the antenna operates as an efficient radiator.

The 2D-radiation patterns are measured at two principle cut planes ($\phi=0°$ and $\phi=90°$) at 6.8, 6.92, 7.1 GHz in the far-field region. The measured cross-polar level is observed below -12 dB in the E-plane and -15 dB in H-plane at all three resonant frequencies which are close to the simulated counterparts. The average simulated front-to-back ratio (FTBR) level is observed better than 18 dB, while the measured value is 14 dB at each resonant frequency in both the E- and H-planes, respectively.

It is evident from Fig. 6 that the proposed geometry shows a unidirectional radiation pattern due to cavity-backed structure and maximum radiation is oriented towards the boresight direction. It can be observed from Fig. 6, the measured 2D radiation pattern response closely follows the simulation response at each resonant frequency in all the directions in both E- and H-planes. To illustrate the best part of the geometry, the performance of the
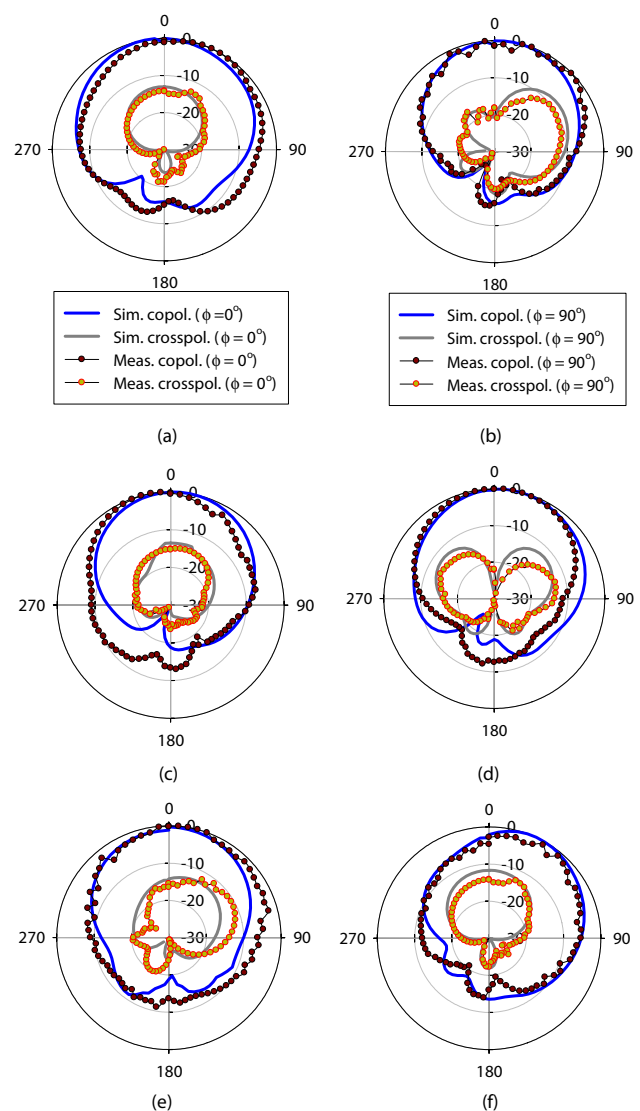

Fig. 6 Simulated and measured radiation patterns for H-plane ($\phi=0°$) and E-plane ($\phi=90°$) **a** at 6.8 GHz, **b** at 6.92 GHz, and **c** at 7.1 GHz

proposed antenna has been compared with other reported works [6–28] in Table 1. The proposed design shows a higher value of gain compared to other geometries except [27], however, the proposed antenna shows better bandwidth. The size of the proposed antenna is more compact than other prototypes, except [11, 14]. However, the antenna presented in [14] has approx. 50% lower bandwidth than the proposed geometry. The proposed antenna is more compact, low profile, exhibiting better bandwidth and uniform radiation characteristics than other existing works, presented in Table 1. Moreover, the proposed dual T-shaped slot antenna is a single-layered that makes it highly capable to integrate with any planar circuit. Moreover, the functionality of the proposed antenna design can

Table 1 Comparison of proposed geometry with existing literature

Param	f_r (GHz)	Peak gain (dBi)	Substrarte (dB)/thickness (h)	Band-width (%)	Size in (electrical length)
[6]	10	5.4	Rogers 5880/05	1.7	$1.2\,\lambda_1 \times 0.89\,\lambda_1$
[7]	5.8	6.2	Rogers 5880/1.57	6.0	$1.1\,\lambda_1 \times 1.3\lambda_1$
[11]	9.84, 8.27	6	Rogers 5880/0.5	6.3	$0.91\,\lambda_1 \times 0.77\,\lambda_1$
[14]	2.46	5.8	Rogers 5880/1.57	3.3	$0.78\,\lambda_1 \times 0.7\,\lambda_1$
[22]	5.8	3.8	Rogers 5880/1.57	6.1	$1.1\,\lambda_1 \times 0.5\lambda_1$
[23]	14.5, 15.7	4	Rogers 5880/1.57	13	$1.1\,\lambda_1 \times 1.5\,\lambda_1$
[27]	5.8	3.12	Felt/1	3.9	$1.6\,\lambda_1 \times 1.0\,\lambda_1$
[28]	5.7, 5.85	7.15	RO 4003C./1.524	5.2	$0.9\,\lambda_1 \times 1.2\,\lambda_1$
This work	6.8, 7, 7.2	6.5	Rogers 5880/1.57	6.2	$0.86\,\lambda_1 \times 0.86\,\lambda_1$

$^a\lambda_1$ is the guiding wavelength at the fundamental mode

be extended by employing active glazing unit with photovoltaic modules and for energy harvesting application [31–34]. As a future scope, the proposed design can be implemented by using new and advanced materials like platinum-free photoelectrochromic materials, biopolymer material, Nano Silver Wire and photovoltaic materials, etc. [35–37]. Implementation of the design with novel materials could have potential applications for light-harvesting antenna with a photosystem photovoltaic device [38]. The proposed design can be integrated easily on the roof of the car/vehicle by computer numerical control (CNC) machining technology [39]. Therefore, the large integrated ground plane, including metallic roof hinders the backside radiation which leads even better performance in terms of the harveting energy for sustainable development.

4 Conclusion

A single-layered, simple, and compact size antenna is presented for bandwidth enhancement. The conventional cavity features are achieved in a planar profile by employing SIW technology. A dual T-shaped slot antenna is engraved in the top cladding of the cavity for radiation and a shorting via is inserted between the slots for bandwidth enhancement. By optimizing the dimensions of the slot and location of the via, the distributed circuit element values are varied, thus all the three modes are coupled in the desired frequency band and impedance bandwidth is achieved by 400 MHz. The proposed design shows a better gain, uniform radiation pattern, and comparatively small circuitry size with other existing antennas in the literature. The measured results validate a good matching with simulations. The planar, simple and low profile proposed geometry is a suitable option for a multi-band high data rate wireless communication system.

Declarations

References

1. J.H. Fu, O.H. Raheem, A novel IMSL tunable phase shifter for HMSIW-LWA-fed rectangular patches based on nematic liquid crystal. Appl. Phys. A **123**(7), 1–8 (2017)
2. A. Kumar, S. Imaculate Rosaline, Hybrid half-mode SIW cavity-backed diplex antenna for on-body transceiver applications. Appl. Phys. A **127**(11), 1–7 (2021)
3. A. Kumar, Design of self-quadruplexing antenna using substrate-integrated waveguide technique. Microw. Opt. Technol. Lett. **61**(12), 2687–2689 (2019)
4. A. Kumar, M. Saravanakumar, S. Raghavan, Dual-frequency SIW-based cavity-backed antenna. AEU Int. J. Electron. Commun. **97**, 195–201 (2018)
5. A. Kumar, A.A. Althuwayb, Wideband triple resonance patch antenna for 5G Wi-Fi spectrum. Prog. Electromagn. Res. Lett. **93**, 89–97 (2020)
6. G.Q. Luo, Z.F. Hu, L.X. Dong, L.L. Sun, Planar slot antenna backed by substrate integrated waveguide cavity. IEEE Antennas. Wirel. Propag. Lett. **7**, 236–239 (2008)
7. D. Chaturvedi, S. Raghavan, Circular quarter-mode SIW antenna for WBAN application. IETE J. Res. **64**(4), 482–488 (2018)
8. A. Kumar, S. Raghavan, A review: Substrate integrated waveguide antennas and arrays. J. Telecommun. Electron. Comput. Eng.: JTEC. **8**(5), 95–104 (2016)
9. K. Arvind, S. Raghavan, Design of SIW cavity-backed self-triplexing antenna. Electron. Lett. **54**(10), 611–612 (2018)
10. N.C. Pradhan, K.S. Subramanian, R.K. Barik, Q.S. Cheng, A shielded-QMSIW-based self-diplexing antenna for closely spaced bands and high isolation. IEEE Antennas Wirel. Propag. Lett. **20**(12), 2382–2386 (2021)
11. G.Q. Luo, Z.F. Hu, W.J. Li, X.H. Zhang, L.L. Sun, J.F. Zheng, Bandwidth-enhanced low-profile cavity-backed slot antenna by using hybrid SIW cavity modes. IEEE Trans. Antennas Propag. **60**(4), 1698–2170 (2012)

12. A. Kumar, S. Raghavan, Wideband slotted substrate integrated waveguide cavity-backed antenna for Ku-band application. Microw. Opt. Technol. Lett. **59**(7), 1613–1619 (2017)

13. A. Kumar, S. Raghavan, Bandwidth enhancement of substrate integrated waveguide cavity-backed bow-tie-complementary-ring-slot antenna using a shorted-via. Def. Sci. J. **68**(2), 197–202 (2018)

14. S. Yun, D. Kim, S. Nam, Bandwidth enhancement of cavity-backed slot antenna using a via-hole above the slot. IEEE Antennas Wirel. Propag. Lett. **11**, 1092–1095 (2012)

15. A. Kumar, A.A. Althuwayb, SIW resonator based duplex filtenna. Antennas Wirel. Propag. Lett. **20**, 2544–2548 (2021)

16. A. Kumar, Wideband circular cavity-backed slot antenna with conical radiation patterns. Microw. Opt. Technol. Lett. **62**(6), 2390–2397 (2020)

17. D. Chaturvedi, SIW cavity-backed 24° inclined-slots antenna for ISM band application. Int. J. RF Microw. Comput. Aided Eng. **30**(5), e22160 (2020)

18. A. Kumar, S. Raghavan, A design of miniaturized half-mode SIW cavity backed antenna, in *2016 IEEE Indian Antenna Week (IAW 2016)* (IEEE, 2016), pp. 4–7

19. D. Dashti, M.H. Neshati, Development of low-profile patch and semi-circular SIW cavity hybrid antennas. IEEE Trans. Antennas Propag. **62**(9), 4481–4488 (2014)

20. A. Kumar et al., SIW cavity-backed circularly polarized square ring slot antenna with wide axial-ratio bandwidth. AEU Int. J. Electron. Commun. **94**, 122–127 (2018)

21. A. Kumar, S. Raghavan, Broadband SIW cavity-backed triangular-ring-slotted antenna for Ku-band applications. AEU Int. J. Electron. Commun.. **87**, 60–4 (2018)

22. T. Deckmyn, S. Agneessens, A.C. Reniers, A.B. Smolders, M. Cauwe, D.V. Ginste, H. Rogier, A novel 60 GHz wideband coupled half-mode/quarter-mode substrate integrated waveguide antenna. IEEE Trans. Antennas Propag. **65**(12), 6915–6926 (2017)

23. D. Chaturvedi, A. Kumar, S. Raghavan, A wideband HMSIW based slotted antenna for Wi-Fi application. IET Microw. Antennas Propag. **13**, 258–262 (2018)

24. A. Kumar, M.J. Al-Hasan, A coplanar-waveguide-fed planar integrated cavity backed slotted antenna array using TE 33 mode. Int. J. RF Microw. Comput. Aided Eng. **30**(10), e22344 (2020)

25. K.Z. Hu, M.C. Tang, Y. Wang, D. Li, M. Li, Compact, vertically integrated duplex filtenna with common feeding and radiating SIW cavities. IEEE Trans. Antennas Propag. **69**(1), 502–507 (2020)

26. A. Kumar, S. Raghavan, Broadband dual-circularly polarised SIW cavity antenna using a stacked structure. Electron. Lett. **53**(17), 1171–1172 (2017)

27. Y. Hong, J. Tak, An all textile SIW cavity-backed circular ring slot antenna for WBAN applications. IEEE Antenna Wirel. Propag. Lett. **15**, 1995–1999 (2016)

28. D. Chaturvedi, S. Raghavan, On-body resilient SIW based antenna for WBAN applications, in *IEEE Twenty-Third National Conference on Communications (NCC)* (2017), pp. 1–4

29. Y. Shi, J. Liu, Y. Long, Wideband triple-and quad-resonance substrate integrated waveguide cavity-backed slot antennas with shorting vias. IEEE Trans. Antennas Propag. **65**, 5768–5775 (2017)

30. A.A. Althuwayb, M.A.J. Al-Hasan, A. Kumar, D. Chaturvedi. Design of half-mode substrate integrated cavity inspired dual-band antenna. Int. J. RF Microw. Comput. Aided Eng. **31**(2), e22520 (2021)

31. L. Fagiolari, E. Varaia, N. Mariotti, M. Bonomo, C. Barolo, F. Bella, Poly (3, 4-ethylenedioxythiophene) in dye-sensitized solar cells: toward solid-state and platinum-free photovoltaics. Adv. Sustain. Syst. **5**, 2100025 (2021)

32. A. Kumar, D. Chaturvedi, S. Raghavan, Design of a self-diplexing antenna using SIW technique with high isolation. AEU Int. J. Electron. Commun. **94**, 386–391 (2018)

33. P. Jankowski-Mihułowicz, W. Węglarski, W. Lichoń, M. Chamera, P. Pyt, C. Ciejka, Synthesis of antennas for active glazing unit with photovoltaic modules. Energies **14**(20), 6632 (2021)

34. A. Kumar, D. Chaturvedi, S. Raghavan, Design and experimental verification of dual-fed, self-diplexed cavity-backed slot antenna using HMSIW technique. IET Microw. Antennas Propag. **13**(3), 380–385 (2019)

35. L. Lavagna, G. Syrrokostas, L. Fagiolari, J. Amici, C. Francia, S. Bodoardo, G. Leftheriotis, F. Bella, Platinum-free photoelectrochromic devices working with copper-based electrolytes for ultrastable smart windows. J. Mater. Chem. A **9**, 19687 (2021)

36. N.A. Rahman, S.A. Hanifah, N.N. Mobarak, A. Ahmad, N.A. Ludin, F. Bella, M.S. Su'ait, Chitosan as a paradigm for biopolymer electrolytes in solid-state dye-sensitised solar cells. Polymer **230**, 124092 (2021)

37. J.C. de Haro, E. Tatsi, L. Fagiolari, M. Bonomo, C. Barolo, S. Turri, F. Bella, G. Griffini, Lignin-based polymer electrolyte membranes for sustainable aqueous dye-sensitized solar cells. ACS Sustain. Chem. Eng. **9**(25), 8550–8560 (2021)

38. Y. Takekuma, H. Nagakawa, T. Noji, K. Kawakami, R. Furukawa, M. Nango, N. Kamiya, M. Nagata, Enhancement of photocurrent by integration of an artificial light-harvesting antenna with a photosystem I photovoltaic device. ACS Appl. Energy Mater. **2**(6), 3986–3990 (2019)

39. A. Kumar, D. Chaturvedi, S. Raghavan, Dual-band, dual-fed self-diplexing antenna, in *2019 13th European Conference on Antennas and Propagation (EuCAP)* (IEEE, 2019), pp. 1–5